

ARTICLE

<https://doi.org/10.1038/s41467-019-08804-y>

OPEN

Genesis of electron deficient Pt₁(O) in PDMS-PEG aggregates

Kairui Liu^{1,2}, Guangjin Hou¹, Jingbo Mao^{1,3}, Zhanwei Xu¹, Peifang Yan¹, Huixiang Li¹, Xinwen Guo³, Shi Bai^{4,5} & Z. Conrad Zhang¹

While numerous single atoms stabilized by support surfaces have been reported, the synthesis of in-situ reduced discrete metal atoms weakly coordinated and stabilized in liquid media is a more challenging goal. We report the genesis of mononuclear electron deficient Pt₁(O) by reducing H₂PtCl₆ in liquid polydimethylsiloxane-polyethylene glycol (PDMS-PEG) (Pt₁@PDMS-PEG). UV-Vis, far-IR, and X-ray photoelectron spectroscopies evidence the reduction of H₂PtCl₆. CO infrared, and ¹⁹⁵Pt and ¹³C NMR spectroscopies provide strong evidence of Pt₁(O), existing as a pseudo-octahedral structure of (R¹OR²)₂Pt(O)Cl₂H₂ (R¹ and R² are H, C, or Si groups accordingly). The weakly coordinated (R¹OR²)₂Pt(O)Cl₂H₂ structure and electron deficient Pt₁(O) have been validated by comparing experimental and DFT calculated ¹⁹⁵Pt NMR spectra. The H⁺ in protic state and the Cl⁻ together resemble HCl as the weak coordination. Neutralization by a base causes the formation of Pt nanoparticles. The Pt₁@PDMS-PEG shows ultrahigh activity in olefin hydrosilylation with excellent terminal adducts selectivity.

¹State Key Laboratory of Catalysis, Dalian National Laboratory for Clean Energy, Dalian Institute of Chemical Physics, Chinese Academy of Sciences, 457 Zhongshan Road, 116023 Dalian, Liaoning, China. ²University of Chinese Academy of Sciences, 100049 Beijing, China. ³State Key Laboratory of Fine Chemicals, PSU-DUT Joint Centre for Energy Research, School of Chemical Engineering, Dalian University of Technology, 116024 Dalian, China. ⁴Department of Chemistry and Biochemistry, University of Delaware, Newark, DE 19716, USA. ⁵State Key Laboratory of Applied Organic Chemistry, Lanzhou University, 730000 Lanzhou, Gansu, China. Correspondence and requests for materials should be addressed to Z.C.Z. (email: zc Zhang@dicp.ac.cn) or to S.B. (email: bais@udel.edu)

Supported single atoms have been prepared using various methods^{1,2}. The reduced metal atoms are stabilized on solid surfaces through metal-support interaction^{3,4} or by strong ligand coordination^{5,6}. The noble metal atoms are often capable of activating adsorbed reactants in catalysis^{7,8}. Reduced single atoms tend to aggregate into nanoparticles in liquid media in the absence of strong ligand coordination⁹. Full and strong coordination is not desired for metal catalysts¹⁰. Therefore, synthesis of weakly coordinated and yet stable metal atoms in liquid media may pave a new path for facile preparation of highly dispersed metal catalysts by overcoming the long-standing challenge of metal aggregation. The readily removable ligands from the discrete metal atoms may also potentially enable atomically controllable synthesis of metallic materials by design.

Numerous surfactants with diverse functionalities have been used in the synthesis of metallic nanoparticles^{11,12} or metal ion-surfactant complexes^{13,14} in micro-emulsions system. The synthesis of discrete reduced metal atoms with weak coordination, which are sufficiently stable in storage at moderate temperature has not been reported. In this work, we chose polydimethylsiloxane-polyethylene glycol (PDMS-PEG) copolymer as an amphiphilic solvating agent. The hydrophilic and semicrystalline PEG blocks enable the dispersion of the hydrophobic PDMS blocks in aqueous solutions^{15,16}. In our synthesis, ethanol is used as the reductant for Pt(IV)^{17,18}, in the presence of optimized 10% (v/v) water to accelerate the rate of reduction⁹, while the diverse oxygen-containing functionality of PDMS-PEG offer weak coordination to the Pt atoms.

Results & discussion

Formation and spectroscopic characterizations of Pt₁(0) in ethanol reduction of ionic Pt precursors. Weakly coordinated mononuclear Pt₁(0) (Pt₁@PDMS-PEG) was prepared by ethanol reduction of H₂PtCl₆ in PDMS-PEG/ethanol–water (see Methods). The characteristic ultraviolet (UV)–visible (Vis) absorption peak of [PtCl₆]²⁻ at 265 nm disappeared and that of [PtCl₄]²⁻ anions at 220 nm was absent^{17,18} after the solution was refluxed for 3 h at 105 °C, indicating complete reduction of the Pt ions (Fig. 1a). While the decrease of the signal at 329 cm⁻¹ in far infrared spectra^{19,20} (Fig. 1b) confirmed the loss of Coulombic Pt–Cl bonds, characterized by the chlorides of positively charged Pt ions, the retained Cl with a Cl/Pt atomic ratio of 2 in Pt₁@PDMS-PEG was determined by chloride ion-chromatography analysis (Supplementary Table 1). Concomitant with the reduction of Pt(IV) (Supplementary Table 2), the color of the solution turned from bright yellow to colorless. Furthermore, the characteristic broad peak of Pt nanoparticles between 400 and 800 nm was not observed (Fig. 1a),

indicating the absence of Pt_n clusters in the system²¹. When PDMS-PEG was replaced by either PDMS or PEG alone, a dark brown color indicative of Pt nanoparticle formation was observed under the same conditions¹⁸.

The absence of ¹⁹⁵Pt nuclear magnetic resonance (NMR) signals near 0 ppm^{22,23} for [PtCl₆]²⁻ and –1617 ppm²⁴ for [PtCl₄]²⁻ confirms the full reduction of platinum. Meanwhile, a pronounced ¹⁹⁵Pt NMR peak at –2680 ppm (Fig. 2a1) was observed and assigned to Pt₁(0) in PDMS-PEG. This conclusion has been independently verified by the reduction of [PtCl₄]²⁻ in PDMS-PEG monitored by ¹⁹⁵Pt NMR (Supplementary Fig. 1). ¹⁹⁵Pt NMR calculation of Pt(II) in PtCl₂L₂ or binuclear Pt₂(μ-Cl)₂Cl₂L₂ complexes with bridging Cl ligands (Supplementary Table 3) also supports the reduced state of Pt₁ center²⁵.

CO has been widely used to probe the dispersion of Pt particles on supports⁴. CO is known to coordinate to Pt by forming a linear Pt–CO bond or bridged bonds (Pt₂CO and Pt₃CO) on the surface of Pt clusters⁴. The identity of the discrete mononuclear state of Pt atoms was further verified by CO coordination using ¹⁹⁵Pt and ¹³C NMR spectroscopy. ¹³CO treatment of Pt₁@PDMS-PEG (Methods) led to an up-field shift of the ¹⁹⁵Pt peak from –2680 to –3231 ppm as a doublet with a splitting of 1750 Hz, (Fig. 2b1), corresponding to one CO coordination to one Pt₁(0) center. The ¹³C NMR spectrum (Fig. 2b2) of this sample also showed a new peak at 150.4 ppm with a ¹⁹⁵Pt satellite doublet (¹⁹⁵Pt–¹³CO) having the same splitting (1750 Hz). Since the ¹³C NMR chemical shift of solvated CO in various solvents ranges from 184.9 to 188.0 ppm²⁶, the peak at 150.4 ppm can be assigned to the carbon of the newly formed Pt•••C=O species. In concert with the experimental observation, the density functional theory (DFT) calculation of ¹³C NMR chemical shift also shows a 24.1 ppm up-field shift from the gas phase CO to Pt•••C=O (Entries 8, 13 in Supplementary Table 4).

In both ¹⁹⁵Pt and ¹³C NMR spectra, the splitting of 1750 Hz can be unambiguously assigned as the spin–spin coupling constant ¹J(¹⁹⁵Pt–¹³C). ¹³CO coordination to any form of multi-nuclear platinum cluster would produce more complex spin–spin coupling patterns than a simple doublet (Fig. 2b) of a linear Pt•••C=O structure. Thus, we conclude that the observed ¹⁹⁵Pt NMR data unambiguously demonstrate the discrete mononuclear state of Pt atoms and Pt₁•••C=O species, respectively.

When a concentrated Pt₁@PDMS-PEG solution was purged with CO (Methods), a new peak at 341 cm⁻¹ (vibration of Pt₁–CO) in far infrared appeared^{19,20} (Supplementary Fig. 2). Altogether with the ¹⁹⁵Pt NMR signal shift to –3231 ppm after the ¹³CO treatment, the results indicate that CO is a strong ligand. The

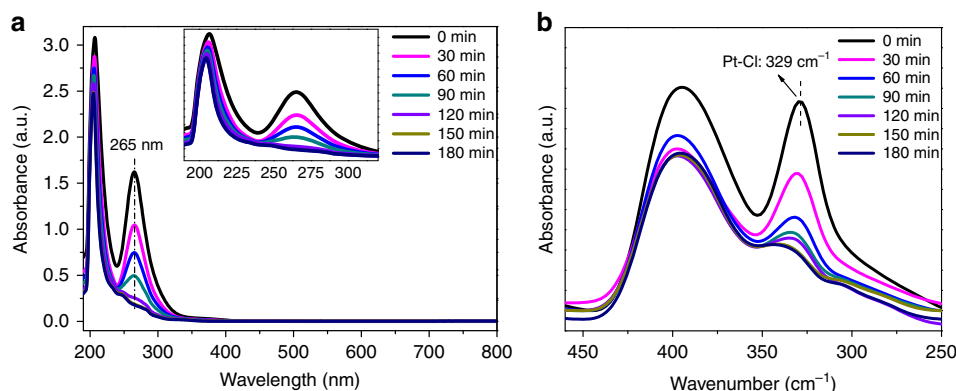


Fig. 1 The reduction of H₂PtCl₆. **a** Ultraviolet (UV)–visible (Vis) spectra of H₂PtCl₆ during the ethanol reduction process. **b** Far infrared spectra in the process of H₂PtCl₆ reduction

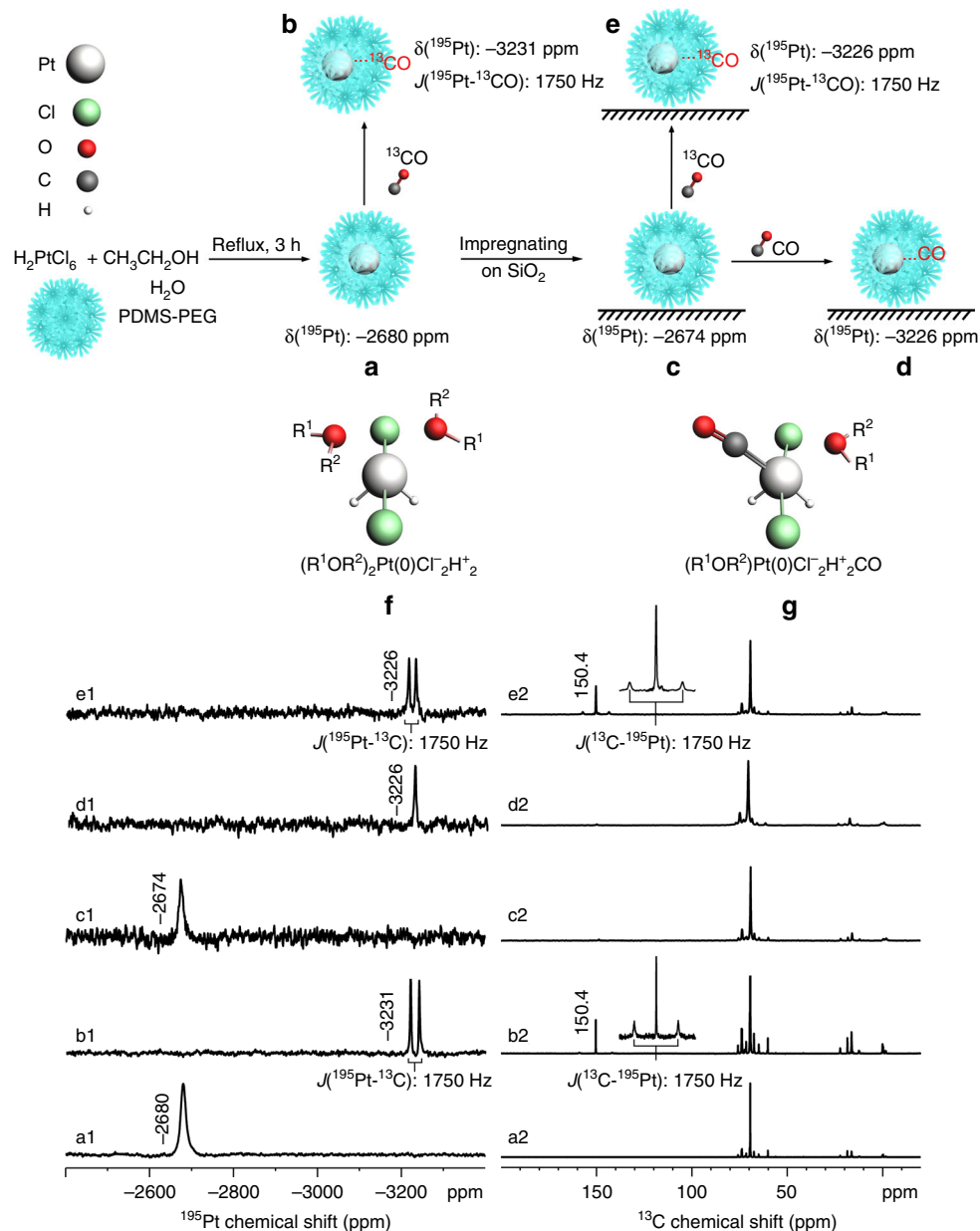


Fig. 2 ^{195}Pt NMR (a1–e1) and corresponding ^{13}C NMR (a2–e2) spectra of **a** Pt_1 @PDMS-PEG liquid; **b** ^{13}CO treated Pt_1 @PDMS-PEG liquid; **c** 2 wt% Pt_1 @PDMS-PEG/ SiO_2 ; **d** CO treated 2 wt% Pt_1 @PDMS-PEG/ SiO_2 ; **e** ^{13}CO treated 2 wt% Pt_1 @PDMS-PEG/ SiO_2 . Note: 2 wt% refers to the Pt loading on SiO_2 ; **f**, **g** are the selected density functional theory (DFT) models of *pseudo* octahedral structure of $(\text{R}^1\text{OR}^2)_2\text{Pt}(\text{O})\text{Cl}_2\text{H}^+_2$ (R^1 , R^2 are H, C, or Si groups) and $(\text{R}^1\text{OR}^2)\text{Pt}(\text{O})\text{Cl}_2\text{H}^+_2\text{CO}$ in polydimethylsiloxane-polyethylene glycol (PDMS-PEG), respectively. Note: the sketch only serves as an illustration of possible local structures

^{195}Pt NMR linewidth of 265 Hz for $\text{Pt}_1\cdots\text{C}=\text{O}$, almost fivefold reduction from that of solvated Pt_1 @PDMS-PEG, may be attributed to the enhanced mobility in the vicinity of Pt sites upon formation of the $\text{Pt}\cdots\text{C}=\text{O}$ bond.

Determination of coordination structure and electronic state of $\text{Pt}_1(\text{O})$. Extensive DFT-based structure screening using geometry optimization was followed by validation through comparing the calculated ^{195}Pt chemical shifts of the selected structural models^{27–29} with the experimental shifts. Consistent with the fact that there are two chlorines per $\text{Pt}_1(\text{O})$ in Pt_1 @PDMS-PEG based on the chloride ion chromatographic analysis, the DFT survey reveals a set of *pseudo* octahedral

structures $(\text{R}^1\text{OR}^2)_2\text{Pt}(\text{O})\text{Cl}_2\text{H}^+_2$ (R^1 , R^2 are H, C, or Si groups) (Entries 2–5, Supplementary Table 4) that not only stabilize $\text{Pt}_1(\text{O})$, but also leads to the calculated ^{195}Pt chemical shifts in reasonable agreement with the experimental value (–2680 ppm) for Pt_1 @PDMS-PEG.

In general, these structures contain two electron-donating oxygens (hydroxyl oxygens of water, ethanol as well as ester oxygens of siloxane and PEG segments) and an otherwise *cis*-divacant octahedral structure ($\text{Pt}_1\text{H}_2\text{Cl}_2$) (Entry 1, Supplementary Table 4). The DFT calculation indicates the coordination of $\text{Pt}_1(\text{O})$ by H, Cl, and O simultaneously prevents $\text{Pt}_1(\text{O})$ from forming aggregates. We noted that various oxygen coordinated structures, excluding Cl and H and the structures in which H^+ bound to Cl^- failed to produce a structure matching the observed ^{195}Pt

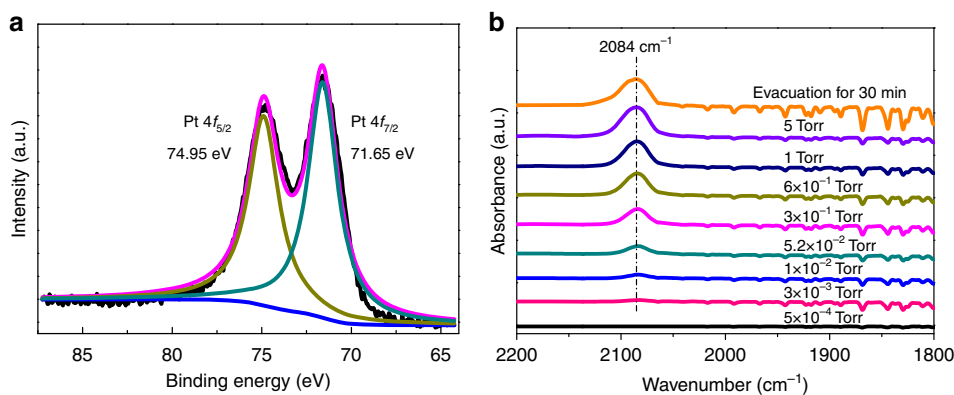


Fig. 3 X-ray photoelectron spectra and CO adsorption of Pt₁(0) atoms. **a** X-ray photoelectron spectra of 0.5 wt% Pt₁@PDMS-PEG/SiO₂, and **b** In situ diffuse reflectance infrared Fourier-transform (DRIFT) spectroscopy of CO adsorption on 1 wt% Pt₁@PDMS-PEG/SiO₂

chemical shift (Supplementary Table 4). Moreover, the DFT calculation shows that the Bader charge of Pt atoms in the optimized structures (Entries 1–5, Supplementary Table 4) is around 0.6 eV, indicating the Pt₁(0) atoms are electron deficient (Pt₁^{δ+} ($0 < \delta < 1$)), possibly associated with the partial electronegative charge of Cl⁻. The Bader charge of hydrogen is positive for all optimized (R¹OR²)₂PtCl₂H₂ structures (Entries 2–5, Supplementary Table 4), suggesting the H in (R¹OR²)₂PtCl₂H₂ is similar to labile proton rather than to hydride in nature. In the presence of abundant protons such as in residual H₂O and OH groups of the solvent, the protic H in the (R¹OR²)₂PtCl₂H₂ could be readily hydrated, e.g. H₃O⁺. The calculated ¹⁹⁵Pt chemical shift (−2705 ppm) of (R¹OR²)₂Pt(0)Cl⁻₂(H₃O⁺)₂ (Entry 6, Supplementary Table 4) is in an excellent agreement with the experimental shift (−2680 ppm), suggesting that (R¹OR²)₂Pt(0)Cl⁻₂(H₃O⁺)₂ may exist as a hydrated form of (R¹OR²)₂PtCl⁻₂H⁺₂ in the system. This calculated result is a further validation of the existence of protic H, rather than a hydride. The absence of ¹⁹⁵Pt–H spin–spin couplings in the ¹⁹⁵Pt spectra may be explained by the rapid chemical exchanges between the protic H in (R¹OR²)₂PtCl⁻₂H⁺₂ and abundant labile protons of water and hydroxyl protons in the system. Furthermore, the protic H in the (R¹OR²)₂Pt(0)Cl₂H₂ is consistent with a recent report that showed HCl acted as a weak ligand in the stabilization of Ir nanoparticles with the H in protic state³⁰. The PtCl₂²⁻ species quickly aggregated to form Pt nanoparticles in methanol–water solution⁹. In our system, the (R¹OR²)₂Pt(0)Cl⁻₂H⁺₂ is well stabilized by the PDMS-PEG matrix.

Besides the weak coordination of the dioxygen in the liquid, the (R¹OR²)₂Pt(0)Cl₂H₂ is acidic because of the protic H. We found that the Cl and H in PtCl₂H₂ are readily removable by neutralization with a base, accompanying with the release and subsequent destabilization of bare Pt₁^{δ+} atoms even at ambient temperature. The sintering of Pt under such condition was evidenced by noting the color of the solution changing from colorless to dark brown, which apparently is not associated with Pt(II or IV) chlorides. The fact that no redox reaction occurred during the neutralization process confirmed the Pt₁ in (R¹OR²)₂PtCl₂H₂ was in reduced state. The Pt coordination with H and Cl further verified by HBr exchange, which led an up-field ¹⁹⁵Pt NMR chemical shift of (R¹OR²)₂PtBr⁻₂H⁺₂ to −3399 ppm (Supplementary Fig. 3), as was predicted by the calculated ¹⁹⁵Pt NMR value (−3197 ppm, Entry 7, Supplementary Table 4).

To further verify the *pseudo* octahedral structures with a CO coordination as Pt•••C=O, we replaced one of oxygen-containing groups (R¹OR²) with CO, followed by DFT geometry optimization and ¹⁹⁵Pt NMR chemical shift calculation. The

corresponding optimized structures (Entries 9–12, Supplementary Table 4) yielded the calculated ¹⁹⁵Pt chemical shifts again in acceptable agreement with the experimental value (−3231 ppm) of Pt•••C=O. A model without proper oxygen coordination (Entry 8, Supplementary Table 4) failed to produce ¹⁹⁵Pt chemical shift in conformity to the experimental value. Experimentally, the ¹⁹⁵Pt chemical shift is up-field shifted by 551 ppm from Pt₁@PDMS-PEG to the CO treated Pt₁@PDMS-PEG. ¹⁹⁵Pt chemical shift calculation shows that one CO coordination replacing one of the two R¹OR² coordination (Entries 9–12, Supplementary Table 4) led to an up-field shift ranging from 366 to 489 ppm compared to the corresponding dioxygen coordinated structures (Entries 2–5, Supplementary Table 4), in remarkable agreement with the experimental up-field shift value of 551 ppm. At the same time, replacing the first R¹OR² group with CO is energetically favored ($\Delta E = -0.18$ eV). Further replacement of the remaining R¹OR² with a CO resulted in negligible energy difference ($\Delta E = -0.04$ eV), consistent with fact that only one CO binds to Pt₁^{δ+} atom. DFT calculation also shows that di-coordinated Pt(II) structures, *trans*-Pt(II)Cl₂(CO)₂ and *cis*-Pt(II)Cl₂(CO)₂, could not produce predicted chemical shifts in agreement with the experimentally observed value −3231 ppm (Supplementary Table 5). In addition, unlike (R¹OR²)Pt(0)Cl₂H₂, the formation of dicarbonyl complex, Pt(II)Cl₂(CO)₂, from Pt(II)Cl₂(R¹OR²) is energetically favorable by the DFT calculations (Supplementary Table 5).

To demonstrate the versatility of preparing supported mononuclear electron-deficient Pt from the liquid Pt₁(0) precursor, a Pt₁@PDMS-PEG/SiO₂ sample with Pt loading equivalent to 2.0 wt% with respect to SiO₂ was prepared (see Methods). In comparison, a low Pt loading, e.g., 0.17 wt%, was essential for the direct preparation of Pt single atoms on oxides support⁴ to minimize Pt sintering due to its weak interaction with the support. Solid-state ¹⁹⁵Pt magic angle spinning (MAS) NMR spectrum (Figure 2c1) of the Pt₁@PDMS-PEG/SiO₂ showed a peak at −2674 ppm, resembling that of Pt₁@PDMS-PEG in terms of chemical shift. After CO treatment (see Methods), the ¹⁹⁵Pt peak was shifted up-field to −3226 ppm (Figure 2d1). The same ¹J(¹⁹⁵Pt–¹³C) values were simultaneously observed in the ¹⁹⁵Pt and ¹³C MAS NMR spectra (Figs. 2e1 and e2) upon ¹³CO treatment of the Pt₁@PDMS-PEG/SiO₂ sample, indicating that Pt₁@PDMS-PEG was well preserved and stably dispersed on the silica surface even after “drying” under vacuum at 40 °C. Remarkably, the Pt₁@PDMS-PEG and Pt₁@PDMS-PEG/SiO₂ samples remained stable for over six months in storage at ambient temperature as evidenced by almost identical ¹⁹⁵Pt NMR spectra periodically measured.

To further verify the oxidation state of Pt after the reduction, a Pt₁@PDMS-PEG liquid sample impregnated on pristine SiO₂ was studied by X-ray photoelectron spectroscopy (XPS) (Fig. 3a). A peak at 71.65 eV (Pt 4f_{7/2}), which is 0.45 eV higher than that of bulk Pt metal (71.20 eV)³¹ and 1.55 eV lower than that of Pt(II) (73.20 eV)³², confirmed the reduced state of Pt atoms in Pt₁@PDMS-PEG/SiO₂. Only one infrared (IR) absorption peak at 2084 cm⁻¹ was observed for CO adsorbed on Pt₁@PDMS-PEG/SiO₂, but not on PDMS-PEG/SiO₂ (Supplementary Fig. 4) by in situ diffuse reflectance infrared Fourier-transform (DRIFT) spectroscopy (Fig. 3b). Peak between 1800 and 1900 cm⁻¹ for bridged CO was not observed, and the peak at 2084 cm⁻¹ did not shift with increasing CO pressure, indicating the absence of nanoparticles in the system⁴. The DRIFT result is consistent with the NMR results of CO treated Pt₁@PDMS-PEG (one-to-one coordination between CO and Pt₁^{δ+} center), and the characteristic peaks at 2178 and 2138 cm⁻¹ corresponding to the *cis*-Pt(II) Cl₂(CO)₂ were absent³³.

The morphology of Pt₁@PDMS-PEG solution was characterized by transmission electron microscopy (TEM). Fairly unilamellar vesicles with a narrow distribution (30–80 nm, Supplementary Fig. 5a) were formed³⁴. The energy-dispersive X-ray spectroscopy analysis in a scanning transmission electron microscope (STEM) revealed the existence of Pt in the vesicles (Supplementary Fig. 5b and Supplementary Table 6). It should be noted that the Pt atoms tend to agglomerate under intense electron beam or X-ray radiation, making TEM, STEM, and synchrotron X-ray measurements infeasible in providing unambiguous evidence of discrete Pt atoms in our system³⁵.

Catalytic performance of electron deficient Pt₁(0) in hydrosilylation reactions. An application of Pt₁@PDMS-PEG as demonstrated in this work is its superb performance in hydrosilylation reaction^{36,37}. Pt₁@PDMS-PEG exhibited an ultrahigh activity with high selectivity (99%) to the terminal adduct in the benchmark hydrosilylation reaction of 1-octene and (Me₃SiO)₂-MeSiH (Supplementary Table 7 and Supplementary Fig. 6). No 1-octene conversion was observed in a blank test using PDMS-PEG alone (Supplementary Table 7). The turnover frequency (TOF) of the Pt₁@PDMS-PEG catalyst is 2 to 4 orders of magnitude higher than that of Karstedt³⁸, NHC-Pt complexes^{37,39}, and silylene-Pt complexes^{38,40} (Supplementary Table 7 and Supplementary Fig. 7). The turnover number (TON) exceeded 5.0 × 10⁸ for the hydrosilylation reaction of 1-octene using (Me₃SiO)₂MeSiH as the silylation reagent. Induction period of the hydrosilylation by Pt₁@PDMS-PEG was negligible. The reaction solution remained colorless and transparent throughout hydrosilylation reaction.

The ultrahigh activity of Pt₁@PDMS-PEG catalyst may be attributed to electron deficiency of the Pt₁^{δ+} center⁴¹ and the reversible weakly electron-donating R¹OR² ligands as compared to the 1,3-divinyl-1,1,3,3-tetramethyldisiloxane (dvtms) or other olefin ligands. The Bader charge (~0.6 eV) on the Pt₁^{δ+} center in (R¹OR²)₂PtCl₂H₂ (Entries 2–5, Supplementary Table 4) is much higher than the charge (0.13 eV) for Pt in the tri-olefin coordinated complex (Entry 9, Supplementary Table 8), representing Karstedt Pt catalyst. ¹⁹⁵Pt chemical shift of the Pt₁@PDMS-PEG is about 3450 ppm down-field shifted to that of the Karstedt Pt catalyst⁴², also in conformity with the high electron deficiency of the Pt₁@PDMS-PEG catalyst. The dvtms coordinated Pt catalysts are typically characterized by a relative long induction period partly due to the slow substitution of dvtms by reactants³⁹.

When 1-octene was added to Pt₁@PDMS-PEG, the ¹⁹⁵Pt NMR peak showed an insignificant up-field shifted by only 26 ppm to –2706 ppm (Supplementary Fig. 8). DFT calculation shows that

only mono-olefin complex (olefin)₁(R¹OR²)₁PtCl₂H₂ produces a ¹⁹⁵Pt NMR chemical shift that reasonably agrees with the experimentally observed value (Entry 2, Supplementary Table 8). All structures with multiple olefin coordination fail to predict the experimental ¹⁹⁵Pt NMR chemical shift. The dvtms stabilized Pt catalysts were reported to form colloidal platinum species, accompanied by the change of the solution color to yellow during the hydrosilylation catalysis process^{43,44}, making the nuclearity of the active Pt catalyst debatable. In this work, in addition to the invariant color throughout the hydrosilylation reaction, the ¹⁹⁵Pt NMR of the reaction solution after the catalytic reaction shows that the catalyst remained in mononuclear Pt₁(0) state (Supplementary Fig. 9, *n*_{1-octene}:*n*_{silane} = 5:3), suggesting that the highly durable mononuclear Pt₁(0) center is the active site in Pt₁@PDMS-PEG for the reaction. Moreover, through three recycled uses, Pt₁@PDMS-PEG maintained high activity without noticeable deactivation in 1-octene hydrosilylation with (Me₃SiO)₂MeSiH (Supplementary Fig. 10). The color of the reused Pt₁@PDMS-PEG solution remained clear throughout the reuses.

Conclusion. We prepare discrete Pt₁@PDMS-PEG through ethanol reduction of H₂PtCl₆. UV-Vis, Fourier-transform infrared spectroscopy (FTIR), ¹⁹⁵Pt, and ¹³C NMR and XPS spectroscopies provide strong evidence for the formation of Pt₁(0). Based on the extensive DFT structure screening and by comparing the calculated and experimental ¹⁹⁵Pt NMR chemical shifts, a pseudo octahedral Pt₁(0) structure, (R¹OR²)₂Pt(0) Cl₂H₂ with weakly coordinated Pt₁(0) is proposed. Pt₁@PDMS-PEG shows high thermal stability in solution and on support in a moderate temperature range. As a catalyst, it exhibits ultrahigh activity and durability for hydrosilylation with superb selectivity to terminal adduct. The electron-deficient Pt₁^{δ+} center together with weak oxygen coordination may contribute to the high performance in hydrosilylation. Pt₁@PDMS-PEG could be a potential new generation of hydrosilylation catalyst.

Methods

Chemicals. 1-Octene (98%), silica, and PEG-200 were purchased from Aladdin Industrial Corporation. PDMS-2000 were purchased from Alfa Aesar (China) Chemicals Co., Ltd. *N,N*-dimethylaniline (99%) and 1,1,1,3,3,5,5,5-heptamethyltrisiloxane (98%) were purchased from Tokyo Chemical Industrial Co., LTD. Hydrochloric acid, chloroplatinic acid, ethanol, and ammonium hydroxide were purchased from Sinopharm Chemical Reagent Co., Ltd. PDMS-PEG was purchased from Guangzhou Tinci Materials Technology Co., Ltd. The molecular weight of each block is 30,000 for PDMS and 545 for PEG-12. Ultrapure water purified by Milli-Q Advantage A10 was used.

Sample preparation. Preparation of Pt₁@PDMS-PEG stock solution by reduction of H₂PtCl₆ with ethanol: PDMS-PEG (0.6465 g), ethanol (135 ml), and ultrapure water (10.2 ml) were stirred in a round-bottom flask at 450 rpm at room temperature (RT). After 10 min, 4.8 ml H₂PtCl₆ solution (1.84 × 10⁻² mol l⁻¹) was added, and the mixture was stirred for 10 more minutes. The solution was refluxed at 105 °C for 3 h and then cooled to RT. (For NMR characterization, ethanol and water were evaporated at 40 °C under reduced pressure).

¹³CO treatment of Pt₁@PDMS-PEG: Ethanol and water were removed under vacuum from the Pt₁@PDMS-PEG stock solution at 40 °C. The Pt₁@PDMS-PEG sample was purged with He for 30 min (100 ml min⁻¹), followed by admission of 5% ¹³CO/He (15 ml min⁻¹) for another 30 min. The sample was flushed with He for 1 h to remove free ¹³CO and collected in a glovebox under N₂.

CO treatment of Pt₁@PDMS-PEG for Far-IR (FIR) characterization: Ethanol and water were removed under vacuum from the Pt₁@PDMS-PEG stock solution at 40 °C. The Pt₁@PDMS-PEG sample was purged with He for 30 min (100 ml min⁻¹), followed by admission of 5% CO/He (15 ml min⁻¹) for another 30 min. The sample was flushed with He for 1 h to remove free CO and collected in a glovebox under N₂ before the FIR characterization.

Preparation of Pt₁@PDMS-PEG/SiO₂: A calculated amount of silica based on the desired final Pt loading was added to 150 ml Pt₁@PDMS-PEG stock solution and stirred for 1 h. Ethanol and water were removed at 40 °C under vacuum. The sample was further vacuum dried for 12 h at 40 °C. For DRIFT experiment and

catalytic reactions, the pH value of the Pt₁@PDMS-PEG stock solution was adjusted to 3.2 by NH₃·H₂O solution before the evacuation.

¹³C treatment of Pt₁@PDMS-PEG/SiO₂: In a quartz tube 200 mg Pt₁@PDMS-PEG/SiO₂ was purged with He for 30 min (100 ml min⁻¹) and 5% ¹³CO/He (15 ml min⁻¹) for another 30 min. The sample was flushed with He for 1 h to remove free gas phase ¹³CO and collected in a glovebox under N₂.

1-Octene disposed Pt₁@PDMS-PEG: Concentrated 150 ml Pt₁@PDMS-PEG solution to 20 ml. Added 0.0990 g 1-octene (ten times equivalent to Pt₁) and 6 ml CHCl₃ into the 20 ml concentrated solution (the use of CHCl₃ is to enhance the 1-octene dissolution in the system). Stirred for 24 h at 40 °C and followed by further concentrating the solution to about 3 ml. The sample was collected in a glovebox under N₂ prior to the ¹⁹⁵Pt NMR measurement.

Ultraviolet (UV)-visible (Vis). UV-Vis spectra was collected on a Shimadzu UV-2600 spectrophotometer.

X-ray photoelectron spectra (XPS). The surface composition and the binding energy (B.E.) of the catalyst were determined by XPS on an ESCALAB250 X-ray photoelectron spectrometer with contaminated C as the internal standard (C1s = 284.6 eV).

NMR spectroscopy. All solid-state NMR measurements were carried out on a 11.7 T wide-bore Bruker Avance III solid-state NMR spectrometer, operating at a Larmor frequency of 500.13 MHz for ¹H, 125.77 MHz for ¹³C, and 107.21 MHz for ¹⁹⁵Pt. A 4.0 mm Bruker multinuclear HX double resonance magic angle spinning (MAS) probe was used. The experiments were acquired at 25 °C and an MAS frequency of 10 kHz, controlled to within +/−3 Hz using the Bruker MAS controller. The typical 90° pulse length was 2.5 μs (¹H), 3.6 μs (¹³C), and 4.2 μs (¹⁹⁵Pt). Seventy-six thousand two-hundred scans were collected for ¹⁹⁵Pt MAS NMR spectra with a recycle delay of 1 s and 30° pulse excitation (1.4 us). Eight-thousand one-hundred ninety-two scans were collected for ¹³C MAS NMR spectra with a recycle delay of 3 s, where ¹H SPINAL-64 heteronuclear decoupling with field strength of 90 kHz was applied during the acquisition period. Solution NMR spectra were obtained on Bruker Avance III 600 MHz and 400 MHz using the 5 mm multinuclear probe. Single pulse and proton decoupling were used for ¹⁹⁵Pt and ¹³C measurements with 3-s relaxation delay, respectively. The solution and solid-state ¹⁹⁵Pt NMR spectra were referenced to a platinum peak of a 1.2 M Na₂PtCl₆ D₂O solution. The chemical shifts of ¹H and ²⁹Si NMR spectra were referenced externally to TMS.

Fourier-transform infrared spectroscopy (FTIR). A DiffusIR diffuse reflectance accessory (Pike Technologies) was used for the FTIR measurements. A leveled attenuated total reflectance (ATR) accessory (Pike Technologies) with a 3 mm diameter diamond plate was used for Middle IR (MIR) and FIR measurements. The FIR instrument (Thermo Scientific Nicolet iS50) is equipped with mercury cadmium telluride (MCT) detector and DTGS/polyethylene detector. The DRIFT measurement has a resolution of 4 cm⁻¹ and 64 scans were collected, while for FIR measurements, 128 scans were collected with a resolution of 16 cm⁻¹. For the DRIFT measurements, the sample was evacuated at 25 °C for 1 h before absorption of high purity probing CO gas. For the FIR measurements, a steady flow of nitrogen was maintained and a high-temperature vacuum-grease-sealed glass lid was used above the sample to prevent air and moisture. Before the FIR experiment, ethanol and water in all the samples were removed by evacuation.

Transmission electron microscopy (TEM) and scanning transmission electron microscope (STEM). STEM analyses were performed with a JEOL JEM-2100F microscope operated at 200 kV. TEM analyses were performed with a JEOL JEM-2000EX microscope operated at 120 kV. A few droplets of the stock solution were put on a microgrid carbon polymer supported on a copper grid and allowed to dry out at room temperature for TEM and STEM observations. The samples were evacuated under ultrahigh vacuum for 20 min in the microscope before observations. For TEM characterization, phosphotungstic acid was used as the staining reagent.

Chloride ion analysis by ion-chromatography. A THERMOICIS-5000 ion-chromatography with the Electrochemical Detector (ED) and the AS-11 and AS-22 columns were used for the detection of Cl⁻ in Pt₁@PDMS-PEG. Before detection, a 5 ml of Pt₁@PDMS-PEG was diluted to 10 ml with water to reach an appropriate concentration for ion chromatographic analysis.

Computation of NMR shifts. The Amsterdam Density Functional (ADF) approach⁴⁵, by which the relativistic effects for calculating of chemical shielding of heavy atom such as platinum can be implemented, was used. The relativistic effects were treated in the ADF as all-electron zeroth-order regular approximation (ZORA). For the chemical shielding, the spin-orbital (SO) two-component was used while for the geometry optimization the scalar approximation neglecting SO coupling was utilized. More specifically, as suggested by Autschbach et al.^{27–29}, the

revised Perdew-Burke-Ernzerhof (revPBE) functional was used for all calculations, and the Slate-type of basis sets (TP2Z) were used for ligand atoms and the quadruple-quadruply polarized (QZ4P) ZORA basis was set for Pt, respectively. The calculated chemical shift of the optimized structures was referenced to the calculated isotropic shielding constant ($\sigma^{\text{ref}} = 2005$ ppm) of the reference compound [PtCl₆]²⁻ by the definition of $\delta = (\sigma^{\text{ref}} - \sigma)/(1 - \sigma^{\text{ref}}) \approx (\sigma^{\text{ref}} - \sigma)$ with an assumption that $(1 - \sigma^{\text{ref}}) \approx 1$. The geometry of [PtCl₆]²⁻ was optimized ($d_{\text{Pt-Cl}} = 2.392$ Å) using the same method described above prior to the calculation of the shielding constant (σ^{ref}). Similar ADF method with scalar approximation neglecting SO coupling was used to calculate ¹³C chemical shielding of gas phase CO and Pt-coordinated CO in various structures.

General procedure for hydrosilylation. We followed Iwamoto's procedure³⁸ to evaluate the Pt₁@PDMS-PEG as the catalyst for the hydrosilylation reaction of 1-octene with 1,1,1,3,5,5,5-heptamethyltrisiloxane (Supplementary Table 7). In all, 0.034 ml Pt₁@PDMS-PEG stock solution (Pt concentration of 5.88×10^{-4} mol l⁻¹) was added into the reactor. Ethanol and water were evacuated at RT. All reactions were carried out in glovebox. 1-Octene (4 mmol) was added and mixed with the Pt₁@PDMS-PEG [corresponding to $n(1\text{-octene}):n(\text{Pt}_1) = 200,000:1$] for 3 min at 25 °C before reaction. 1,1,1,3,5,5,5-heptamethyltrisiloxane (4.4 mmol) was then added, and the reaction was carried out at 50 °C. After reaction, 2 mmol N,N-dimethylaniline (0.2424 g) was added as an internal standard. Products and reactants were characterized by ¹H NMR (400 MHz, CDCl₃, and Supplementary Fig. 6). Blank test was run as follows: hydrosilylation reaction was carried out with PDMS-PEG/ethanol-water as the catalyst (without Pt) following the same procedure as for the hydrosilylation of 1-octene catalyzed by Pt₁@PDMS-PEG. No conversion of 1-octene was observed (Supplementary Table 7).

The reported conversion measurement was repeated at least three times under the same condition, and the uncertainty was typically below 5%. The average value of multiple measurements is presented in the paper.

The turnover frequency (TOF), defined as the number of moles of terminal product (T) yield per mole of Pt₁(0) within a unit time, is calculated in unit of h⁻¹ according to

$$\text{TOF} = \frac{n_{\text{T}}}{n_{\text{Pt}}} \times \frac{1}{t} \\ = \frac{n_{\text{olefin},0} \times \text{yield}_{\text{T}}}{n_{\text{Pt}}} \times \frac{1}{t}$$

Since the conversion reached nearly completion in a minute, the initial TOF was calculated by taking t as 1 min for the catalytic reaction under consideration.

$n_{\text{olefin},0}$ is the initial number of moles of 1-octene used in the reaction. Note that $n_{1\text{-octene},0}$ is 4 mmol.

n_{T} is the number of moles of product, T (terminal adduct).

n_{Pt} is the number of moles of Pt added in the reaction.

t is the reaction time. The conversion value was calculated at $t = 1$ min.

$$\text{yield}_{\text{T}} = \text{conversion} \times \text{selectivity}$$

Turnover numbers (TONs). TON of Pt₁@PDMS-PEG in the hydrosilylation reaction between 1-octene and 1,1,1,3,5,5,5-heptamethyltrisiloxane: 0.0068 ml Pt₁@PDMS-PEG stock solution (diluted 10 times, 5.88×10^{-5} mol l⁻¹, 4×10^{-10} mol) was added into the round-bottom flask, followed by evacuation of ethanol-water. All reaction was carried out in glovebox. 1-Octene (40 mmol) was added and mixed with the Pt₁@PDMS-PEG [$n(1\text{-octene}):n(\text{Pt}_1) = 1 \times 10^8:1$] for 3 min at 25 °C before reaction. 1,1,1,3,5,5,5-heptamethyltrisiloxane (48 mmol) was then added, and the mixture was refluxed at 70 °C. After the completion of the reaction (verified by ¹H NMR), add more 1-octene and 1,1,1,3,5,5,5-heptamethyltrisiloxane (1:1.2) into the reactor and continue the reaction.

Catalyst recycle. After the hydrosilylation reaction between 1-octene and (Me₂SiO)₂MeSiH (1-octene: 0.4488 g, (Me₂SiO)₂MeSiH: 0.89 g) finished, the solution was centrifuged. In all, 0.6694 g reaction mixture was taken out from the upper solution, and analyzed by ¹H NMR. The remaining solution (0.6694 g) was used for the subsequent hydrosilylation reaction. For the reuse test, 0.4488 g 1-octene and 0.89 g (Me₂SiO)₂MeSiH was added. After reaction, solution was centrifuged. In all, 1.3388 g (equal to the amount of added reactants) reaction mixture was taken out from the upper solution, and analyzed by ¹H NMR, while the remaining solution (0.6694 g) was used for the subsequent hydrosilylation reaction. For the following reuses, the added amounts of 1-octene and (Me₂SiO)₂MeSiH were always 0.4488 and 0.89 g, respectively. After each reaction, the amount of reaction mixture taken out for ¹H NMR from the upper solution after centrifugation was always 1.3388 g (equal to the amount of added reactants), and the remaining solution was kept at 0.6694 g for the subsequent hydrosilylation reaction.

Data availability

The data that support the findings in this study are in the published article and/or its Supplementary Information files. The whole datasets are available from the

corresponding author on reasonable request. The source data are provided as a Source Data file.

Received: 16 August 2018 Accepted: 29 January 2019

Published online: 01 March 2019

References

1. Wang, A., Li, J. & Zhang, T. Heterogeneous single-atom catalysis. *Nat. Rev. Chem.* **2**, 65–81 (2018).
2. Yang, X.-F. et al. Single-atom catalysts: A new frontier in heterogeneous catalysis. *Acc. Chem. Res.* **46**, 1740–1748 (2013).
3. Flytzani-Stephanopoulos, M. Gold atoms stabilized on various supports catalyze the water-gas shift reaction. *Acc. Chem. Res.* **47**, 783–792 (2014).
4. Qiao, B. et al. Single-atom catalysis of CO oxidation using Pt1/FeOx. *Nat. Chem.* **3**, 634–641 (2011).
5. Wei, S. et al. Direct observation of noble metal nanoparticles transforming to thermally stable single atoms. *Nat. Nanotechnol.* **13**, 856–861 (2018).
6. Liu, W. et al. Discriminating catalytically active FeNx species of atomically dispersed Fe-N-C catalyst for selective oxidation of the C-H bond. *J. Am. Chem. Soc.* **139**, 10790–10798 (2017).
7. Wei, H. et al. FeOx-supported platinum single-atom and pseudo-single-atom catalysts for chemoselective hydrogenation of functionalized nitroarenes. *Nat. Commun.* **5**, 5634 (2014).
8. Liu, W. et al. Single-atom dispersed Co-N-C catalyst: structure identification and performance for hydrogenative coupling of nitroarenes. *Chem. Sci.* **7**, 5758–5764 (2016).
9. Chen, S. et al. Initial reaction mechanism of platinum nanoparticle in methanol-water system and the anomalous catalytic effect of water. *Nano Lett.* **15**, 5961–5968 (2015).
10. Appleton, T. G., Clark, H. C. & Manzer, L. E. The trans-influence: Its measurement and significance. *Coord. Chem. Rev.* **10**, 335–422 (1973).
11. Stubenrauch, C., Wielputz, T., Sottmann, T., Roychowdhury, C. & DiSalvo, F. J. Microemulsions as templates for the synthesis of metallic nanoparticles. *Colloids Surf. A* **317**, 328–338 (2008).
12. Jana, N. R., Gearheart, L. & Murphy, C. J. Seed-mediated growth approach for shape-controlled synthesis of spheroidal and rod-like gold nanoparticles using a surfactant template. *Adv. Mater.* **13**, 1389–1393 (2001).
13. Parera, E., Comelles, F., Barnadas, R. & Suades, J. New surfactant phosphine ligands and platinum(II) metallosurfactants. Influence of metal coordination on the critical micelle concentration and aggregation properties. *Langmuir: ACS J. Surf. Colloids* **26**, 743–751 (2010).
14. de la Iglesia, P., Jaeger, V. W., Xi, Y., Pfaendtnr, J. & Pozzo, L. D. Structure characterization and properties of metal-surfactant complexes dispersed in organic solvents. *Langmuir: ACS J. Surf. Colloids* **31**, 9006–9016 (2015).
15. Kickelbick, G., Bauer, J., Huesing, N., Andersson, M. & Holmberg, K. Aggregation behavior of short-chain PDMS-b-PEO diblock copolymers in aqueous solutions. *Langmuir: ACS J. Surf. Colloids* **19**, 10073–10076 (2003).
16. Schreyeck, G. & Marie, P. Kinetics of the adsorption of a PDMS-g-PEO copolymer at the PDMS/PEO interface. *Langmuir* **15**, 8212–8219 (1999).
17. Wang, S.-R. & Tseng, W. J. Aggregate structure and crystallite size of platinum nanoparticles synthesized by ethanol reduction. *J. Nanopart. Res.* **11**, 947–953 (2009).
18. Chen, C.-W. & Akashi, M. Synthesis, characterization, and catalytic properties of colloidal platinum nanoparticles protected by poly(N-isopropylacrylamide). *Langmuir* **13**, 6465–6472 (1997).
19. Li, H. et al. Isomerization characteristics and the coordination chemistry of metal chlorides in 1-butyl-3-methylimidazolium chloride. *ACS Catal.* **4**, 4446–4454 (2014).
20. Li, H. & Zhang, Z. C. Far reaching potentials of far infrared spectroscopy in catalysis research. *Chin. J. Catal.* **37**, 637–643 (2016).
21. Teranishi, T., Hosoe, M., Tanaka, T. & Miyake, M. Size control of monodispersed Pt nanoparticles and their 2D organization by electrophoretic deposition. *J. Phys. Chem. B* **103**, 3818–3827 (1999).
22. Shelimov, B., Lambert, J. F., Che, M. & Didillon, B. Application of NMR to interfacial coordination chemistry: A Pt-195 NMR study of the interaction of hexachloroplatinic acid aqueous solutions with alumina. *J. Am. Chem. Soc.* **121**, 545–556 (1999).
23. Harris, R. K., McNaught, I. J., Reams, P. & Packer, K. J. Multinuclear high-resolution solid-state magnetic-resonance studies of some platinum(II) complexes with phosphorus-containing ligands. *Magn. Reson. Chem.* **29**, 60–72 (1991).
24. Pellechia, P. J., Gao, J., Gu, Y., Ploehn, H. J. & Murphy, C. J. Platinum ion uptake by dendrimers: An NMR and AFM study. *Inorg. Chem.* **43**, 1421–1428 (2004).
25. Albinati, A., Isaia, F., Kaufmann, W., Sorato, C. & Venanzi, L. M. Solution studies of complexes of the types trans -PtCl2L(1,4-diazine) and trans -LCl2Pt(μ-1,4-diazine)PtCl2L (L = Phosphine, C2H4). X-ray Structures of Pt2Cl4L2 (ppz) (L = C2H4, PEt3; ppz = 2,5-Dimethylpyrazine) and the relative trans influence of alkene and tertiary phosphine ligands. *Inorg. Chem.* **28**, 1112–1122 (1989).
26. Kalodimos, C. G., Gerothanassis, I. P., Pierattelli, R. & Ancian, B. Carbon-13 and oxygen-17 chemical shifts-16O-18O isotope effects on 13C chemical. *Inorg. Chem.* **38**, 4283–4293 (1999).
27. Sutter, K. & Autschbach, J. Computational study and molecular orbital analysis of NMR shielding, spin-spin coupling, and electric field gradients of azido platinum complexes. *J. Am. Chem. Soc.* **134**, 13374–13385 (2012).
28. Autschbach, J. & Le Guennic, B. Solvent effects on 195Pt and 205Tl NMR chemical shifts of the complexes [(NC)5Pt-Tl(CN)n]n- (n = 0–3), and [(NC)5Pt-Tl-Pt(CN)5]3- studied by relativistic density functional theory. *Chemistry* **10**, 2581–2589 (2004).
29. Sterzel, M. & Autschbach, J. Toward an accurate determination of 195Pt chemical shifts by density. *Inorg. Chem.* **45**, 3316–3324 (2006).
30. Mondloch, J. E., Özkar, S. & Finke, R. G. “Weakly ligated, labile ligand” nanoparticles: The case of Ir(0)n-(H + Cl)-m. *ACS Omega* **3**, 14538–14550 (2018).
31. Romeo, M., Majerus, J., Legare, P., Castellani, N. J. & Leroy, D. B. Photoemission-study of Pt Adlayers on Ni(111). *Surf. Sci.* **238**, 163–168 (1990).
32. Bancroft, G. M. et al. ESCA study of sputtered platinum films. *Anal. Chem.* **47**, 586–588 (1975).
33. Bagnoli, F. et al. Halo-carbonyl complexes of platinum(II) and palladium(II). *J. Organomet. Chem.* **622**, 180–189 (2001).
34. Discher, D. E. & Eisenberg, A. Polymer vesicles. *Science* **297**, 967–973 (2002).
35. Ding, K. et al. Identification of active sites in CO oxidation and water-gas shift over supported Pt catalysts. *Science* **350**, 189–192 (2015).
36. Denmark, Scott E. & Wang, Z. Cross-coupling of vinylpolysiloxanes with aryl iodides. *J. Organomet. Chem.* **624**, 372–375 (2001).
37. Marko, I. E. et al. Selective and efficient platinum(0)-carbene complexes as hydrosilylation catalysts. *Science* **298**, 204–206 (2002).
38. Troadec, T. et al. Silacyclopropylideneplatinum(0) complex as a robust and efficient hydrosilylation catalyst. *Inorg. Chem.* **55**, 8234–8240 (2016).
39. Buisine, O. et al. Second generation N-heterocyclic carbene-Pt(0) complexes as efficient catalysts for the hydrosilylation of alkenes. *Chem. Commun.* **0**, 3856–3858 (2005).
40. Iimura, T., Akasaka, N., Kosai, T. & Iwamoto, T. A Pt(0) complex with cyclic (alkyl)(amino)silylene and 1,3-divinyl-1,1,3,3-tetramethyldisiloxane ligands: synthesis, molecular structure, and catalytic hydrosilylation activity. *Dalton Trans.* **46**, 8868–8874 (2017).
41. Chen, Y. et al. Discovering partially charged single-atom Pt for enhanced anti-Markovnikov alkene hydrosilylation. *J. Am. Chem. Soc.* **140**, 7407–7410 (2018).
42. Meister, T. K. et al. Platinum catalysis revisited-unraveling principles of catalytic olefin hydrosilylation. *ACS Catal.* **6**, 1274–1284 (2016).
43. Markó, I. E. et al. Highly active and selective platinum(0)-carbene complexes. Efficient, catalytic hydrosilylation of functionalised olefins. *Adv. Synth. Catal.* **346**, 1429–1434 (2004).
44. Stein, J., Lewis, L. N., Gao, Y. & Scott, R. A. In Situ determination of the active catalyst in hydrosilylation reactions using highly reactive Pt(0) catalyst precursors. *J. Am. Chem. Soc.* **121**, 3693–3703 (1999).
45. Baerends, E. J. et al. Basic Aspects of Density Functional Theory. in *Computational Methods in Catalysis and Materials Science: An Introduction for Scientists and Engineers*. eds van Santen, R. & Sautet, P. (Wiley, New Jersey, 2009).

Acknowledgements

This work was supported by the “Global Expert” program funding of China and by the State Key Laboratory of Catalysis, Dalian Institute of Chemical Physics, Chinese Academy of Sciences. Professors Ulrich Mueller-Westerhoff of University of Connecticut, Mayfair Kung and Harold Kung of Northwestern University offered helpful suggestions in the revision of the manuscript. S.B. and Z.C. thank Professors Cecil Dybowski and Andrew Teplyakov (University of Delaware) for the helpful discussion on the characterization of subnano platinum particles using ¹⁹⁵Pt NMR spectroscopy and the DFT calculations of the model structures. The ¹⁹⁵Pt and ¹³C NMR measurements at University of Delaware were made possible by the Delaware COBRE program, supported by a grant from the National Institute of General Medical Sciences—NIGMS (5 P30 GM110758-02) from the National Institutes of Health.

Author contributions

Z.C.Z. conceived, designed, and led the study. K.L. designed and performed bulk of the experiments in synthesis, characterization and catalytic reactions. J.M. and X.G.

conducted preliminary synthesis and characterization. S.B. and G.H. carried out NMR measurements and analysis of the NMR results. S.B. and K.L. carried out the DFT calculations on the model structures. Z.X. assisted K.L. in analyzing the NMR results of hydrosilylation reaction. P.Y. assisted K.L. in the IR study and chloride ion analysis by ion-chromatography. H.L. assisted K.L. in the far-IR study.

Additional information

Supplementary Information accompanies this paper at <https://doi.org/10.1038/s41467-019-08804-y>.

Competing interests: The authors declare no competing interests.

Reprints and permission information is available online at <http://npg.nature.com/reprintsandpermissions/>

Journal peer review information: *Nature Communications* thanks the anonymous reviewers for their contribution to the peer review of this work. Peer reviewer reports are available.

Publisher's note: Springer Nature remains neutral with regard to jurisdictional claims in published maps and institutional affiliations.



Open Access This article is licensed under a Creative Commons Attribution 4.0 International License, which permits use, sharing, adaptation, distribution and reproduction in any medium or format, as long as you give appropriate credit to the original author(s) and the source, provide a link to the Creative Commons license, and indicate if changes were made. The images or other third party material in this article are included in the article's Creative Commons license, unless indicated otherwise in a credit line to the material. If material is not included in the article's Creative Commons license and your intended use is not permitted by statutory regulation or exceeds the permitted use, you will need to obtain permission directly from the copyright holder. To view a copy of this license, visit <http://creativecommons.org/licenses/by/4.0/>.

© The Author(s) 2019